OR Spectrum (2011) 33:751–786
DOI 10.1007/s00291-011-0249-0

REGULAR ARTICLE

A predictive decision-aid methodology for dynamic mitigation of influenza pandemics

Andrés Uribe-Sánchez · Alex Savachkin · Alfredo Santana · Diana Prieto-Santa · Tapas K. Das

Published online: 7 May 2011

Abstract In a recent report, the Institute of Medicine has stressed the need for dynamic mitigation strategies for pandemic influenza. In response to the need, we have developed a simulation-based optimization methodology for generating dynamic predictive mitigation strategies for pandemic outbreaks affecting several regions. Our methodology can accommodate varying virus and population dynamics. It progressively allocates a limited budget to procure vaccines and antivirals, capacities for their administration, and resources required to enforce social distancing. The methodology uses measures of morbidity, mortality, and social distancing, which are translated into the costs of lost productivity and medical services. The simulation model was calibrated using historic pandemic data. We illustrate the use of our methodology on a mock outbreak involving over four million people residing in four major population centers in Florida, USA. A sensitivity analysis is presented to estimate the impact of changes in the budget availability and variability of some of the critical parameters of mitigation strategies. The methodology is intended to assist public health policy makers.

Keywords Pandemic influenza · Mitigation · Dynamic · Vaccination · Antiviral · Social distancing

1 Motivation

Pandemic influenza (PI) outbreaks have historically caused significant societal and economic disruptions. Since 2003, scattered outbreaks of the *avian-to-human*

A. Uribe-Sánchez · A. Savachkin (✉) · A. Santana · D. Prieto-Santa · T. K. Das
Department of Industrial and Management Systems Engineering, University of South Florida, 4202 E. Fowler Avenue, ENB118, Tampa, FL 33620, USA
e-mail: alexs@usf.edu

transmittable H5N1 virus have been occurring throughout Asia, the Pacific region, Africa, Europe, and the Near East (Centers for Disease Control and Prevention 2008). As of December 2009, the World Health Organization (WHO) has reported 447 cases of confirmed avian-to-human transmission of H5N1 virus resulting in 263 deaths worldwide (World Health Organization 2010a). Although *human-to-human* transmission of H5N1 has so far been reported for a few isolated cases, a mutation of this virus leading to a broader human-to-human transmission presents a threat to our quality of life. A milder human-to-human transmissible H1N1 virus subtype surfaced in Mexico in the Spring of 2009 and propagated to a global H1N1 pandemic outbreak. As of late December 2009, 208 countries were affected with a total number of deaths of at least 11,516 (World Health Organization 2010b). Most experts believe that the next pandemic will likely be caused by a highly pathogenic virus for which we have little or no pre-existing immunity (Schoenstadt 2009).

Mitigating an influenza pandemic requires an understanding of the evolution of the virus and population dynamics during the outbreak. The practicality and effectiveness of mitigation strategies also depend on the available emergency response infrastructure, mitigation resources, and resource allocation policies. With the available technology, even after a new virus subtype is identified, a surge production of adequate vaccine stockpile can take up to 9 months (Fedson and Hant 2003; Aunins et al. 2000). This may limit the use of vaccine as an effective mitigation resource in the critical early stage of a pandemic. Even in the best case scenario, when the emerged virus subtype has a known epidemiology, the existing vaccine stockpile will be insufficient (World Health Organization 2009; WHO Global Influenza Programme 2009). Furthermore, the supply of antiviral drugs, immunizers, healthcare providers, hospital beds, and logistics will also be constrained. The challenge of developing feasible and effective mitigation strategies, attested by the H1N1 2009 outbreak, has been acknowledged by WHO (WHO Global Influenza Programme 2009) and echoed by national public health authorities, including the US Centers for Disease Control and Prevention (CDC; Centers for Disease Control and Prevention 2007a; US Department of Health & Human Services 2007).

2 Status of current literature

The existing general literature on pandemic modeling aims to address various aspects of the pandemic process including (a) underlying spatio-temporal structure, (b) contact mechanism, (c) disease transmission, (d) disease natural history, and (e) development of containment and mitigation strategies. These aspects are closely interrelated. For instance, the nature of the spatio-temporal structure, including composition of the social mixing groups and temporal dynamics of the affected population, drives the contact process which is the main determinant of the disease transmission (Larson 2007; Halloran et al. 2002; Ferguson et al. 2006; Wu et al. 2006b). A comprehensive decision-aid model for containment and mitigation must take into account all of the above constituents; it must incorporate the mechanism of disease progression, from initial infection, to asymptomatic earlier phase, symptom manifestation, and final health outcome (recovery or death)

(Handel et al. 2009; Pourbohloul et al. 2009; Atkinson and Wein 2008); it must also consider the population dynamics of disease spread, including individual susceptibility (Pitzer et al. 2007a,b), transmissibility (Handel et al. 2009; Yang et al. 2007, 2009a; Cauchemez et al. 2004), and human behaviors that mediate infection generation (Colizza et al. 2006; Epstein et al. 2007, 2008; Halloran 2006); finally, it must incorporate the impact of pharmaceutical and non-pharmaceutical prevention and intervention, including vaccination, antiviral therapy, social distancing, school and workplace closures, travel restrictions, and use of low-cost measures, such as face masks and hand washing (Longini et al. 2004; Wu et al. 2006b; Atkinson and Wein 2008; Yang et al. 2009b; Tang et al. 2006; Scharfstein et al. 2006; Glass et al. 2006; Lipsitch et al. 2007; Nigmatulina and Larson 2009). In essence, effective mitigation strategies have a twofold objective: (a) systemically to alter the disease dynamics and control disease progression with available clinical therapies, and (b) to alter the social dynamics and contain disease propagation within the affected communities. Mitigation strategies vary in the composition of the target groups, geo-spatial coverage, and implementation time.

The current literature on assessment and development of PI containment and mitigation strategies can be broadly classified into (a) statistical models, (b) mathematical models, (c) simulation-based approaches, and (d) combinations of thereof. In what follows, we present a summary survey of these approaches, mostly focusing on the simulation-based approaches.

The statistical models, driven mainly by likelihood or regression-based approaches, have primarily been used for epidemiological parameter assessment and estimation of the pandemic impact (Cauchemez et al. 2004; Longini and Koopman 1982; Longini 1986). Traditionally, these models have inherently featured relatively simple and general spatio-temporal structures (e.g., homogeneous social mixing groups, Yang et al. 2007; Ball and Lyne 2002; Fraser et al. 2004; Carrat et al. 2005).

The mathematical models have mostly focused on modeling virus spread and policy assessment. Notable examples of such models are dynamic compartmental approaches, typically represented in the form of a set of differential equations, which delineate transitions between disease phases (e.g., susceptible, exposed, symptomatic infected, etc., Larson 2007; Arino et al. 2006; Dargatz et al. 2006; Ferguson et al. 2003). Based on the solution approach, the mathematical models can be subdivided into analytical (or closed form) and iterative. Compared to the statistical models, the dynamic-iterative models feature more granular composition of the mixing groups (Larson 2007; Nigmatulina and Larson 2009; Wu et al. 2006a). However, the degree of granularity is still limited since any additional spatio-temporal considerations can negatively impact the computational robustness of the models. Description of the contact processes in mathematical models generally does not take into account changes in the behavioral patterns during the course of the pandemic (e.g., compliance to intervention by vaccination and social distancing, Arino et al. 2006; Dargatz et al. 2006; Ferguson et al. 2003). Consideration of behavioral aspects can be found in some of the recent simulation-based models (Kelso et al. 2009; Halder et al. 2010; Yasuda and Suzuki 2009; Milne et al. 2008). Furthermore, mathematical models are typically based on the infection pathways and disease progression that are invariant to time and individual attributes (Dargatz et al. 2006; Ferguson et al. 2003).

The simulation-based approaches have been used for modeling virus spread and assessment and generation of pharmaceutical and/or non-pharmaceutical interventions. Based on the way of generating disease progression, these models can be categorized as those that track infection pathway of each individual entity (Longini et al. 2004; Ferguson et al. 2005, 2006; Das and Savachkin 2008; Germann et al. 2006; Patel et al. 2005; Savachkin et al. 2010b) and the rest that are driven by occurrence of infection events (Wu et al. 2006b; Glass et al. 2006). In contrast to the statistical and mathematical models, the simulation models are capable of providing most detailed description of population dynamics whereby each individual can be assigned a set of attributes (e.g., age, gender, community, etc.) that can be modified without altering the general model structure (Das and Savachkin 2008; Uribe et al. 2008). However, such comprehensive descriptive granularity is achieved at the expense of higher data demand and substantial computational burden. As a result, most existing simulation-based approaches incorporate statistical and/or mathematical submodels (e.g., for infection generation) in order to attain an effective balance between model accuracy and practicality (Das and Savachkin 2008; Savachkin et al. 2010b).

In recent years, the simulation-based models have focused on integration of therapeutical and non-therapeutical prevention and intervention, to develop synergistic strategies aimed at result-oriented use of constrained resources. These approaches first aim to implement a form of social distancing to reduce the contact between the susceptible and the infected. The infected population is then treated with an antiviral therapy to reduce infectiousness, and the susceptible is vaccinated to increase their immunity. For example, Wu et al. (2006b) implemented social distancing for all contacted and symptomatic cases followed by antiviral application. Such strategies, which appear to be more discriminating and thus less expensive, have been found to be particularly efficient for low transmissibility scenarios (i.e., scenarios with the values of the basic reproduction number below 1.8, Ferguson et al. 2005; Mills et al. 2004).

Most notable among recent efforts is a 2006–2007 initiative by MIDAS, the Models of Disease Infectious Agent Study network, which studied three independent simulation models (Halloran et al. 2008). These models were used to emulate large-scale PI spread for rural areas of Asia (Ferguson et al. 2005; Longini et al. 2005), US and UK (Ferguson et al. 2006; Germann et al. 2006), and the city of Chicago (Eubank et al. 2004). MIDAS cross-validated the models by simulating the city of Chicago, with 8.6M inhabitants, and implementing targeted layered containment (TLC). Under TLC, the symptomatic infectious cases refrain from going to work (take liberal leave), receive antiviral treatment, and become subject to household quarantine; the asymptomatic contacts receive targeted antiviral prophylaxis (TAP) and become subject to household quarantine. The research findings of the MIDAS network and other institutions (Atkinson and Wein 2008; Glass et al. 2006) were used in a recent "Modeling Community Containment for Pandemic Influenza" report by the Institute of Medicine (IOM), US, to formulate a set of recommendations for mitigating PI at the local level (Committee on Modeling Community Containment for Pandemic Influenza 2006). These recommendations were used in a pandemic preparedness guidance developed jointly by CDC, HHS, and other federal US agencies (Centers for Disease Control and Prevention 2007b).

The IOM report (Committee on Modeling Community Containment for Pandemic Influenza 2006) points out several limitations of the MIDAS models, observing that "because of the significant constraints placed on the models" being considered by policy makers, "the scope of models should be expanded." The IOM recommends that "steps be taken now to adapt or develop decision-aid models that can be readily linked to surveillance data to provide real-time feedback during an epidemic. Research protocols should be developed, approved, and put in place now to generate the information needed during an outbreak to inform models, and improve their disease sub-models." The report also strongly recommends (1) "that future modeling efforts incorporate broader outcome measures ... to include the costs and benefits of intervention strategies", and (2) "that models examining the potential effectiveness of school and workplace closures on mitigating pandemic influenza include a broader range of closure options." We add here that most current approaches focus on assessment of policies defined a priori; few of the existing models for design of synergistic mitigation strategies are "learning", i.e., capable of predicting of and adapting to changes in the course of a pandemic, and ultimately generating a dynamic optimal strategy (Savachkin et al. 2010b). Furthermore, the majority of the current simulation models feature a single-region design (see Appendix Table 1). In Savachkin et al. (2010b), we developed a simulation-based optimization model for generating mitigation strategies for cross-regional pandemic outbreaks. The model was implemented on a sample outbreak and the resultant strategy was compared to the existing governmental pro-rata distribution policy, which allocates mitigation resources to each affected region in proportion to its population (HHS 2007).

In this paper, we present a novel decision-aid methodology for developing dynamic predictive mitigation strategies for a network of regional pandemic outbreaks. The methodology is driven by a large-scale simulation-based dynamic optimization model that incorporates varying virus epidemiology and region-specific population dynamics. The model generates mitigation strategies for an efficient, progressive allocation of limited resources, including stockpiles of vaccines and antiviral drugs, healthcare capacities for administration of vaccination and antiviral therapy, and social distancing enforcement resources. The optimization control seeks dynamically to minimize the impact of ongoing outbreaks and the expected impact of potential outbreaks, and allocates the resources accordingly. The methodology considers measures of morbidity, mortality, and social distancing, translated into the cost of lost productivity and medical expenses (societal and economic costs). The model was calibrated using historic pandemic data and tested on a sample cross-regional outbreak in Florida, USA, with over four million inhabitants. We also present a sensitivity analysis for estimating the marginal impact (measured in terms of the average total pandemic cost and the average number of fatalities) of changes in the total budget availability and variability of some critical decision factors. These factors included: (a) vaccine efficacy, (b) efficacy of antiviral therapy, (c) social distancing conformance level, (d) social distancing declaration threshold, and (e) social distancing period.

Compared to our previous work in Savachkin et al. (2010b), this paper features the following main advances: (a) in Savachkin et al. (2010b), progressive resource allocations are irrevocable, i.e., once resources are allocated to an affected region, they remain in the region until full depletion, regardless of the posterior dynamics of

the overall pandemic; in contrast, our model is capable of re-allocating the resources remaining from the previous distributions, based on the current pandemic status, and thus achieving a more efficient resource utilization; (b) our model incorporates the cost of the resources (e.g., vaccines, antiviral, etc.) and strives to allocate a total available budget, as opposed to a separate allocation of total available quantities of individual resources, which vary significantly in their relative cost and effectiveness; (c) our model investigates optimal policy generation under two scenarios of virus severity: low transmissibility and high transmissibility, as opposed to a high transmissibility analysis in Savachkin et al. (2010b); (d) our study attempts to analyze the effect of social distancing policies (namely, the target population conformance) on the dynamics of societal and economic costs; (e) in this paper, we also present a short description of our decision-aid simulation software made freely available to general public through our web site.

This paper has the following organization. In Sect. 3, we present our simulation-based optimization methodology, including description of the population dynamics and disease transmission, the mechanism of disease progression, and therapeutical and non-therapeutical intervention, followed by description of the calibration methodology for single-region and cross-regional simulation models, and presentation of the optimization control model. In Sect. 4, results of the testbed implementation are presented, followed by discussion of the sensitivity analysis. Conclusions are given in Sect. 5.

3 Simulation-based optimization model

Our large-scale simulation-based optimization model generates predictive strategies to allocate a total available budget of mitigation resources over a network of regional pandemic outbreaks, progressively, from one affected region to the next. Mitigation resources include stockpiles of vaccine(s) and antiviral drug(s), hospital beds, capacities for vaccination and antiviral administration, social distancing enforcement resources, among others. The methodology combines a cross-regional simulation model, a set of single-region simulation models, and an overarching dynamic optimization control.

The regions inside the network are classified as unaffected, ongoing outbreak (which includes new outbreak), and contained (see Fig. 1). The regions are interconnected by air and land travel, which is emulated by the cross-regional model. The single-region model mimics the population and disease dynamics inside each ongoing region, impacted by available pharmaceutical and non-pharmaceutical prevention and intervention. The pandemic spreads from ongoing to unaffected regions by infectious travelers who pass through regional border control. At every new regional outbreak episode (epoch), the cross-regional model invokes the optimization control, which allocates the total available resource budget, including remaining resources from the previous allocations, to the new/ongoing outbreak regions (*actual allocation*) and potential (unaffected) outbreak regions (*virtual allocation*). The objective function of the optimization model incorporates measures of morbidity, mortality, and social distancing, translated into the cost of lost productivity and medical expenses. The

Fig. 1 Schematic of simulation-based optimization methodology

objective function strives to minimize the total cost of the new/ongoing outbreaks and the expected cost of the potential outbreaks, spreading from the ongoing regions. Detailed daily pandemic statistics are collected for each affected region, including the numbers of new infected, deceased, and quarantined cases, for different age groups. As the regional outbreaks become contained, the model estimates their actual societal and economic costs.

In the remainder of this section, we present the details of the cross-regional simulation model (Sect. 3.1) and the single-region simulation model (Sect. 3.2), including the description of the calibration methodology (Sect. 3.3). The dynamic optimization control model is presented in Sect. 3.4, followed by analysis of the results of the testbed implementation in Sect. 4.

3.1 Cross-regional simulation model

The cross-regional simulation model emulates propagation of the pandemic across the network of affected regions. It controls a set of single-region simulation models of ongoing outbreaks and invokes the optimization model for actual and virtual resource allocation at every new outbreak epoch. The schematic of the cross-regional simulation model is presented in Fig. 2.

The model is initialized by generating mixing groups and population dynamics for each network region (for details, see Sect. 3.2.1). A pandemic is triggered by injecting one or more infectious cases into a randomly selected region, designated as the initial outbreak region. Details associated with the resulting contact dynamics and disease propagation within the region are presented in Sect. 3.2. As the symptomatic cases start seeking medical assistance, the new regional outbreak is detected.

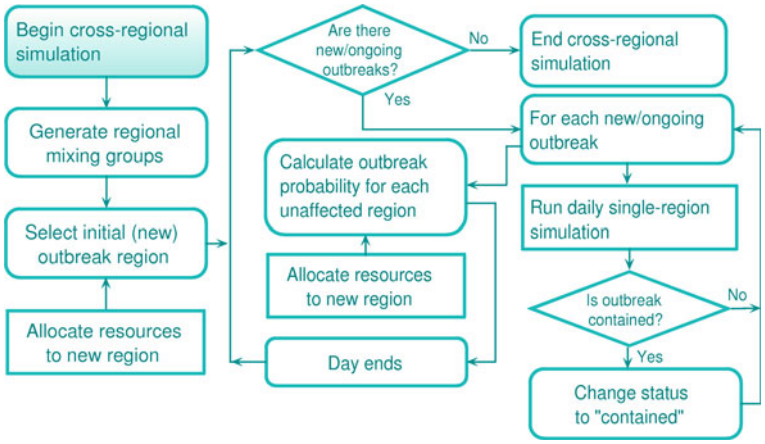

Fig. 2 Schematic of cross-regional simulation model

At this point, the model calls the optimization control which generates a resource allocation (see Sect. 3.4). The cross-regional simulation then passes control back to the single-region model, which executes a cycle (e.g., daily) of the regional disease and population dynamics, now mediated by the allocated clinical therapies and social distancing measures (see Sect. 3.2). The simulation clock inside the single-region routine advances in smaller time increments (e.g., hourly; see Sect. 4).

As the outbreak intensifies, it spreads over to the unaffected regions, as infectious travelers pass undetected through air and land border control with some probability (the probabilities are different for asymptomatic and symptomatic cases). Travelers are considered to act independently. Each infectious traveler is assumed to initiate a regional outbreak with an equal, time-homogeneous probability ω for the entirety of his/her infection period, regardless of his/her point of origin. For each unaffected region, the outbreak probability at time $t > 0$, P_t, is calculated using the binomial probability law as follows:

$$P_t = 1 - (1 - \omega)^{n_t}, \tag{1}$$

where n_t denotes the number of infectious travelers in the region at time t. Based on the outbreak probability value, the cross-regional model determines which of the unaffected regions have become new outbreaks (in the testbed implementation, the values of P_t were computed once at the end of each day). The model also determines if an outbreak has been contained, based on a certain threshold of the daily infection rate. The cross-regional simulation ends when all outbreaks have been contained.

3.2 Single-region simulation model

The single-region simulation model emulates population and disease dynamics within an affected region.

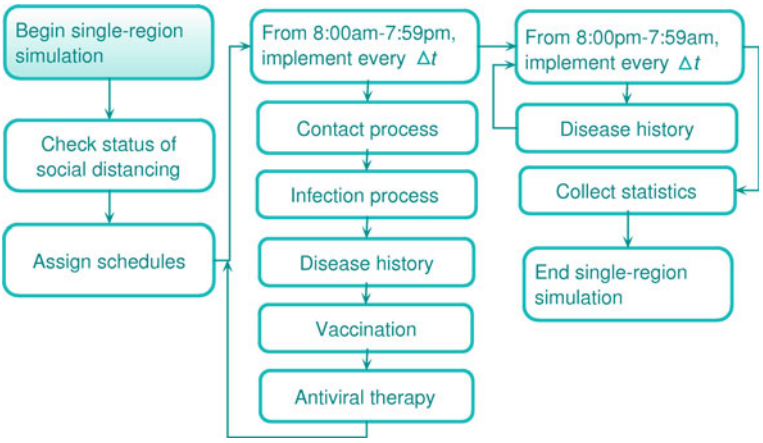

Fig. 3 Schematic of single-region simulation model

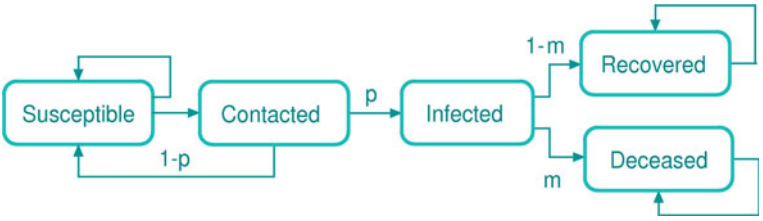

Fig. 4 Schematic of the disease progression model

A schematic of the model is shown in Fig. 3. The model subsumes the following main components: (a) population dynamics, (b) contact and infection process, (c) disease natural history, and (d) mitigation prevention and intervention, including measures of social distancing, vaccination, and antiviral application. The model collects detailed regional influenza statistics, including numbers of infected, recovered, deceased, and quarantined cases, for different age groups. For a contained outbreak, its societal and economic costs are calculated. The societal cost includes the cost of lost lifetime productivity of the deceased; the economic cost includes the cost of medical expenses of the recovered and deceased and the cost of lost productivity of the quarantined (see Sect. 4.1.3). The single-region simulation model builds upon a prototype presented in Das and Savachkin (2008).

At any point of time, the population of an ongoing region is assumed to be composed of the following exclusive compartments: susceptible, contacted, infected, recovered, and deceased (see Fig. 4).

During the course of his/her social interaction, a susceptible individual may periodically come into contact with infectious cases. The contacted individual then either becomes infected with a certain probability p or returns to the compartment of susceptibles. An infected case then either dies with a certain probability m or recovers. It is further assumed that a recovered person develops immunity and cannot be susceptible again. All recovered cases continue circulating through the mixing groups. In what

follows, we present the details of the main components of the single-region simulation model.

3.2.1 Population dynamics

We model a region as a set of population centers composed of *mixing groups* of various types, including households, offices, manufacturing facilities, universities, schools, churches, shopping centers, entertainment centers, etc. A household consists of household members, each of which is assigned a comprehensive set of attributes including age, gender, parenthood, workplace, immunity status, infection susceptibility, probability of travel, and others. Each inhabitant is also assigned Δt time-discrete (e.g., $\Delta t = 1$ h) weekday and weekend schedules, which depend on a number of factors including: (a) age and parenthood, (b) inhabitant's disease status, (c) travel status, (d) social distancing decrees in place, and (e) inhabitant's conformance to them. As their schedules advance, inhabitants circulate throughout the mixing groups, staying a certain amount of time in each of them.

3.2.2 Contact and infection processes

Disease transmission occurs through contact events between infectious and susceptible individuals within the mixing groups. At the beginning of each period Δt (e.g., 1 h), for each mixing group g, the simulation model tracks the total number of infectious cases n_g present in the group. Each infectious case randomly generates r_g per Δt unit of time *new contacts*, uniformly, from the susceptible cases present in the mixing group. We assume the following simplifying characterization of the contact process: (a) during Δt period, a susceptible may come into contact with at most one infectious case and (b) each contact exposure lasts Δt units of time. Once a susceptible has started a contact exposure at time t, he/she will develop into an infectious case at time $t + \Delta t$ with a certain probability that is calculated as shown below.

Let $L_i(t)$ be a nonnegative continuous random variable that represents the duration of contact exposure, starting at time t, that is required for a contact i to become infected. We assume that $L_i(t)$ follows an exponential distribution with parameter $\lambda_i(t)$, where $\lambda_i(t)$ represents the instantaneous force of infection applied to contact i at time t (Wu et al. 2006a; Lawless and Lawless 1982; Diekmann and Heesterbeek 2000). The probability that a susceptible i, whose contact exposure has started at time t, will develop into an infectious case at time $t + \Delta t$ is then given as

$$P\{L_i(t) \leq \Delta t\} = 1 - \mathrm{e}^{-\lambda_i(t)\Delta t}. \tag{2}$$

3.2.3 Disease natural history

It is assumed that upon becoming infected, an individual enters simultaneously into the phases of latency and incubation (see Fig. 5). During the incubation phase, the individual stays asymptomatic (i.e., shows no visible symptoms). At the end of the latency phase, the individual becomes infectious and enters the infectious phase (Germann et al. 2006; Halloran et al. 2008; Longini et al. 2005; Bootsma and Ferguson 2007).

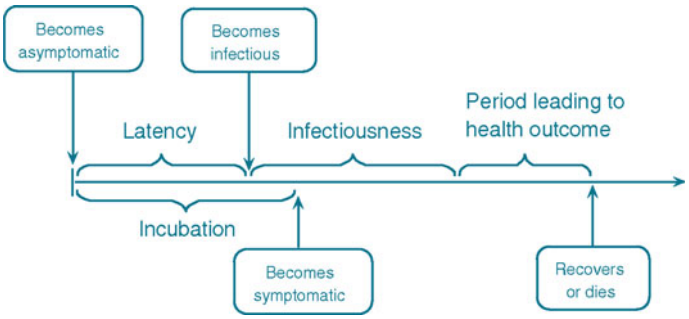

Fig. 5 Schematic of disease natural history model

At the end of the incubation period, the individual becomes symptomatic. At the conclusion of the infectious period, the individual enters the final disease stage which culminates in his/her recovery or death.

Mortality for influenza like diseases is a complex process, which is affected by a number of factors and variables. For most of these variables, little or no accurate data have been collected from past pandemics. In addition, the time of death could oftentimes be weeks following the disease episode (mainly attributable to subsequent pneumonia-related complications, Brundage and Shanks 2008). Because of the uncertainty underlying the mortality process, we adopted a simplified, age-based form of the mortality probabilities, where the mortality probability of infected i, m_i is given as

$$m_i = \mu_i - \tau\rho_i, \tag{3}$$

where μ_i is the age-dependent base mortality probability of infected i, ρ_i is his/her status of antiviral treatment (0 or 1), and τ is the efficacy of the antiviral therapy, measured in terms of the reduction in the base mortality probability (Longini et al. 2005).

3.2.4 Mitigation strategies

Mitigation prevention and intervention considered in the single-region model include pharmaceutical and non-pharmaceutical measures. Implementation of the mitigation measures is initiated upon detection of the first confirmed infected case (Centers for Disease Control and Prevention 2006). At this point, mitigation resources are assigned (see Sect. 3.4) and deployed in the region. The model considers a certain outbreak detection delay and a delay for deployment of field responders.

Pharmaceutical mitigation Pharmaceutical prevention and intervention consist of vaccination and antiviral application. Vaccines are offered to the individuals from a prespecified risk group, to reduce their infection susceptibility. It is assumed that a certain fraction of the risk group will not comply with vaccination. Once administered, the vaccine takes a certain period to become effective (typically, between 10 and 14 days, Pasteur 2009). Vaccination is constrained by the available stockpile and the administration capacity, measured in terms of the number of immunizer-hours.

For antiviral application, we assume that a certain fraction of symptomatic infected cases will seek medical assistance (Blendon et al. 2008; Sadique et al. 2007). Those of them who belong to a prespecified mortality risk group receive an antiviral treatment, to reduce their mortality probability (see Eq. 3). It is assumed that an antiviral becomes effective immediately. The antiviral application is subject to availability of the antiviral stockpile and the administration capacity, measured in terms of the number of certified nurses. Both the antiviral application and vaccination are affected by a number of social behavioral factors, including conformance of the target population, its degree of risk perception, and associated compliance of healthcare personnel (Maunder et al. 2003; Robertson et al. 2004; Pearson et al. 2006). The conformance level of the target population could be affected by the demographical profile of the region (Keane et al. 2005; Niederhauser et al. 2001; Rhodes and Hergenrather 2002; Rosenthal et al. 1995; Smailbegovic et al. 2003) and quality of the public information available (Colorado Department of Human Services Division of Mental Health 2009), among other factors. The degree of risk perception of the target population could be impacted by a negative experience developed during pharmaceutical campaigns of the previous outbreaks (Safranek et al. 1991; Cummings et al. 1979) as well as by public fear and rumors (The New Yorker 2009; The New York Times 2009).

Non-pharmaceutical mitigation For a social distancing mediation, we adopted a guidance suggested by CDC, USA (Centers for Disease Control and Prevention 2007b). The guidance establishes five categories of pandemic severity (from 1 to 5) and recommends different quarantine and closure policies for each of the categories. The categories are determined based on the value of the case fatality ratio (CFR), the cumulative proportion of the number of fatalities in the total infected population. Our simulation model periodically reassesses the CFR value during the pandemic course. For the CFR values lower than 0.1% (which corresponds to Category 1), voluntary at-home isolation of the infected cases is *implemented*. If the CFR falls in the range between 0.1 and 1.0% (Categories 2 and 3), in addition to the above at-home isolation, the following measures are *recommended*: (a) voluntary quarantine of households members of infected cases and (b) child and adult social distancing. Finally, for the CFR values exceeding 1.0% (Categories 4 and 5), all the above measures are *implemented*. Alike pharmaceutical measures, the effectiveness of social distancing mitigation is also affected by several of the behavioral factors mentioned above (Colorado Department of Human Services Division of Mental Health 2009). Our model considers a certain social distancing conformance level, which can vary based on the demographics profile. Travel restrictions considered in the model included regional air and land border control for outgoing infected travelers (for details, see the testbed implementation in Sect. 4).

3.3 Calibration methodology

The single-region simulation model was calibrated using two commonly accepted measures of pandemic severity: the *basic reproduction number* (R_0) and the *infection attack rate* (IAR). R_0 is defined as the average number of secondary infections, produced by a typical infected case in a totally susceptible population. Our model with

its a detailed, person-to-person infection generation traceability allows identification of all secondary infections created by each infected case. All infected cases are then classified by generation of infection, as in Glass et al. (2006) and Ferguson et al. (2005), where a generation is defined as the set of all infected cases (offsprings) that are at the same tier of descent from their infection generators (ancestors) (Diekmann and Heesterbeek 2000). The value of R_0 is then calculated as the average reproduction number of a typical generation in the early stage of the pandemic when no interventions are implemented (known as the *baseline* scenario). Our model was calibrated to attain the baseline values of R_0 similar to those obtained from historic pandemic data (Ferguson et al. 2005; Mills et al. 2004; see Sect. 4.1.2).

IAR is defined as the ratio of the total number of infections over the pandemic period to the size of the initial susceptible population. To further calibrate our model, we used the following relationship between baseline R_0 and IAR, as presented in Wu et al. (2006b) and Diekmann and Heesterbeek (2000):

$$R_0 = \frac{-\ln(1 - \text{IAR})}{\text{IAR}}, \quad \text{for } R_0 \geq 1,\ 0 < \text{IAR} < 1. \tag{4}$$

Section 4.1.2 of this paper provides the details of the calibration process for a sample testbed scenario.

3.4 Optimization model

The optimization model is invoked at every new outbreak epoch to allocate the total available resource budget, including remaining resources from the previous allocations, to the new/ongoing outbreak regions (*actual allocation*) and potential outbreak regions (*virtual allocation*). By doing so, the model seeks to progressively minimize the impact of ongoing outbreaks and the expected impact of potential outbreaks. Mitigation resources include stockpiles of vaccine(s) and antiviral drug(s), hospital beds, capacities for vaccination and antiviral administration, social distancing enforcement resources, among others. The objective function of the optimization model incorporates measures of morbidity, mortality, and social distancing, translated into the cost of lost productivity and medical expenses. In what follows, we present the details of the model. We introduce the following notation.

S = the set of all regions,
A^n = the set of regions in which pandemic is contained at the nth outbreak epoch ($n = 1, 2, \ldots$),
B^n = the set of ongoing regions at the nth outbreak epoch,
C^n = the set of unaffected regions at the nth outbreak epoch,
M^n = budget availability at the nth outbreak epoch,
R = the set of available types of mitigation resources ($R = \{1, 2, \ldots, r\}$),
c_i = unit cost of type i resource, $i \in R$,
$\hat{q}_i^n$ = amount of resource i remaining from previous allocations, at the nth outbreak epoch.

Let TC_k^n denotes the total cost of an outbreak in region k at the nth outbreak epoch. The total cost is a function of the *decision variables* q_{ik}^n which denote the amount of resource i allocated to region k at the nth outbreak epoch. We assume that outbreaks occur one at a time. At the nth new outbreak epoch in region j, the following optimization problem is invoked

$$\begin{aligned}
\text{Min} \quad & \mathrm{TC}_j^n(q_{1j}^n, q_{2j}^n, \ldots, q_{rj}^n) + \sum_{l \in B^n \setminus \{j\}} \mathrm{TC}_l^n(q_{1l}^n, q_{2l}^n, \ldots, q_{rl}^n) \\
& + \sum_{s \in C^n} \mathrm{TC}_s^n(q_{1s}^n, q_{2s}^n, \ldots, q_{rs}^n) \cdot p_s^n \\
& \text{subject to} \\
& \sum_{i \in R} c_i \cdot q_{ij}^n + \sum_{l \in B^n \setminus \{j\}} \sum_{i \in R} c_i \cdot q_{il}^n + \sum_{s \in C^n} \sum_{i \in R} c_i \cdot q_{is}^n \cdot p_s^n - \sum_{i \in R} c_i \cdot \hat{q}_i{}^n \leq M^n \\
& q_{ij}^n + \sum_{l \in B^n \setminus \{j\}} q_{il}^n + \sum_{s \in C^n} q_{is}^n \cdot p_s^n \geq \hat{q}_i^n, \quad \forall i \in R.
\end{aligned}$$

In the above objective function, the first term represents the total cost of the new outbreak in region j, estimated at the nth outbreak epoch, and based on the actual resource allocation $\{q_{1j}^n, q_{2j}^n, \ldots, q_{rj}^n\}$. The second term represents the total cost of ongoing outbreaks, excluding region j, which is (re)estimated at the nth outbreak epoch, based on the current pandemic status (for details, see below). This cost is a function of the allocation $\{q_{1l}^n, q_{2l}^n, \ldots, q_{rl}^n\}$, which may include amounts remaining from previous allocations. The third term represents the total expected cost of outbreaks in currently unaffected regions, based on the virtual allocation $(q_{1s}^n, q_{2s}^n, \ldots, q_{rs}^n)$ and the regional outbreak probabilities p_s^n.

The first model constraint relates the total available budget with the value of the current actual and virtual resource allocations, adjusted with the value of the resources remaining from the previous allocations. The second set of constraints guarantees that the needs of the current actual and virtual allocations will first be satisfied using the resources remaining from the previous allocations (the outstanding resource needs will then be fulfilled from the remaining budget).

The total cost of an outbreak in region k at the nth outbreak epoch is calculated as follows:

$$\begin{aligned}
\mathrm{TC}_k^n = & \sum_{h \in \mathcal{H}} (m_h + \bar{w}_h) X_{hk}^n + \sum_{h \in \mathcal{H}} \bar{w}_h \cdot Y_{hk}^n + \sum_{h \in \mathcal{H}} \hat{w}_h \cdot D_{hk}^n + \sum_{h \in \mathcal{H}} w_h \cdot V_{hk}^n \\
& + \sum_{h \in \mathcal{H}} \hat{m}_h \cdot U_{hk}^n, \qquad (5)
\end{aligned}$$

where

$\mathcal{H}$ = the set of age groups,

m_h = total medical cost of an infected case in age group h over his/her disease period,

$\hat{m}_h$ = total medical cost of an uninfected case in age group h over the pandemic period,
$\bar{w}_h$ = total cost of lost wages of an infected case in age group h over his/her disease period,
$\hat{w}_h$ = cost of lost lifetime wages of a deceased case in age group h,
w_h = daily cost of lost wages of a non-infected case in age group h who complies with quarantine,
X^n_{hk} = total number of infected cases in age group h who seek medical assistance,
Y^n_{hk} = total number of infected cases in age group h who do not seek medical assistance,
D^n_{hk} = total number of deceased cases in age group h,
V^n_{hk} = total number of person-days of cases in age group h who comply with quarantine,
U^n_{hk} = total number of uninfected cases in age group h.

Variables X^n_{hk}, Y^n_{hk}, D^n_{hk}, V^n_{hk}, and U^n_{hk} are defined for region k at the nth outbreak epoch. We determine the value of X^n_{hk} using the following regression model

$$X^n_{hk} = \delta^0_{hk} + \sum_{i \in R} \delta^i_{hk} \cdot q_{ik} + \sum_{i,m \in R, i \neq m} \delta^{im}_{hk} \cdot q_{ik} \cdot q_{mk}, \tag{6}$$

where $\delta^i_{\cdot\cdot}$ denotes the regression coefficient associated with resource i, and $\delta^{im}_{\cdot\cdot}$ is the regression coefficient for the interaction between resources i and m. Similar expressions are used for Y_{hk}, D_{hk}, and V_{hk}. U^n_{hk} is obtained by subtracting X^n_{hk} from the total population of the region at the nth outbreak epoch.

We have that $p^n_k = \sum_{l \in B^n} p^n_{lk}$, where p^n_{lk} denotes the outbreak probability in region k, caused by an ongoing outbreak in region l, estimated at the nth outbreak epoch. This probability is considered to be a function of the resource allocation for region l at the nth outbreak epoch, and is calculated using the following regression model:

$$p^n_{lk} = \gamma^0_{lk} + \sum_{i \in R} \gamma^i_{lk} \cdot q_{il} + \sum_{\substack{i,m \in R \\ i \neq m}} \gamma^{im}_{lk} \cdot q_{il} \cdot q_{ml}, \tag{7}$$

where $\gamma^i_{\cdot\cdot}$ denotes the regression coefficient associated with resource i, $\gamma^{im}_{\cdot\cdot}$ is the regression coefficient associated with interaction between resources i and m, and $\gamma^0_{\cdot\cdot}$ represents the intercept.

3.5 Simulation optimization algorithm

Below we present the algorithm for the simulation optimization model.

1. Estimate regression equations for all regions using the single-region simulation model (Eqs. 6, 7).
2. Set $n = 1$. Initialize sets of regions: $A^n = \emptyset$, $B^n = \emptyset$, $C^n = S$.
3. Select randomly the initial outbreak region j.
4. Update sets of regions: $B^n \leftarrow B^n \cup \{j\}$ and $C^n \leftarrow C^n \backslash \{j\}$.

5. Solve the resource allocation model for region j. Update the total budget availability.
6. If $B^n \neq \emptyset$, do Step 7. Else, do Step 9.
7. (a) For each ongoing region, implement a next day run of its single-region simulation.
   (b) Check the containment status of each ongoing region. Update sets A^n and B^n, if needed.
   (c) For each unaffected region, calculate its outbreak probability.
   (d) Based on the outbreak probability values, determine if there is a new outbreak region(s) j. If there is no new outbreak(s), go to Step 6. Otherwise, go to Step 8.
8. For each new outbreak region j,
   (a) Increment $n \leftarrow n + 1$.
   (b) Update sets $B^n \leftarrow B^n \cup \{j\}$ and $C^n \leftarrow C^n \backslash \{j\}$.
   (c) Re-estimate regression equations for each region $k \in B^n \cup C^n$ using the single-region simulations, where each simulation is initialized to the current outbreak status in the region.
   (d) Determine the remaining availability of the previously allocated resources.
   (e) Solve the resource allocation model for each region $k \in B^n$.
   (f) Update the total budget availability.
9. Calculate the total cost (Eq. 5) for each contained region and update the overall pandemic cost.

4 Testbed illustration

A sample cross-regional outbreak scenario included a network of four counties in Florida, USA: Hillsborough, Miami Dade, Duval, and Leon, with populations of 1.0, 2.2, 0.8, and 0.25 million people, respectively. The H5N1 virus subtype was considered. A basic unit of time Δt for people's schedules, contact dynamics, infection transmission, disease natural history, and implementation of interventions was taken to be 1 h (see Fig. 3; Eq. 2). Each regional simulation was run for a period (up to 185 days) until the number of new daily infections approached near zero (see Sect. 4.1.3).

4.1 Model parameter values

This section presents the details on selecting parameter values for cross-regional and single-region models, including parameters of population and disease dynamics, calibration, and mitigation.

4.1.1 Parameters of population and disease dynamics

Demographic and social dynamics data for each of the regions were extracted from the US Census (US Census Bureau 2000) and the National Household Travel Survey (Bureau of Transportation Statistics 2002; Savachkin et al. 2010a; see Appendix Tables 2, 3, 4). Compositions of the regional mixing groups are shown in Appendix Tables 5, 6, 7, 8 (Savachkin et al. 2010a). In these tables, columns 1 and 2 show

the mixing group type and the number of mixing groups for each type, respectively. Column 3 shows the probability distribution among the types for assigning the workplaces of inhabitants. Columns 4–6 show the probability distribution among the types for assigning the weekday after-work errands, weekend errands, and errands during quarantine (see Sect. 4.1.3), respectively. The last column contains the hourly contact rates for each mixing group type. The hourly schedules (Savachkin et al. 2010a) were adopted from Das and Savachkin (2008).

Each infected individual was assigned a daily travel probability of 0.24% (Bureau of Transportation Statistics 2002), of which 7% was by air and 93% by land transportation. The origin-destination travel probabilities within the network of four regions were calculated based on the traffic volume data (Tampa International Airport 2010; Miami International Airport 2010; Jacksonville Aviation Authority 2010; Tallahassee Regional Airport 2010; see Appendix Table 9). Infection detection probabilities for regional border controls for symptomatic cases were assumed to be 95 and 90% (Ortutay 2010), for air and land transportation, respectively. These values were reduced by 70% for asymptomatic travelers (Ortutay 2010). Travel bans were implemented for all detected infectious cases. An undetected infectious traveler was assumed to trigger a regional outbreak in his/her destination with a time-homogeneous probability $\omega = 0.001$ during his/her infectiousness period. The regional outbreak probabilities P_t were calculated once at the end of each day using Eq. 1.

The instantaneous force of infection applied to contact i at time t ($\lambda_i(t)$ in Eq. 2) was modeled as

$$\lambda_i(t) = -\ln(1 - p_i(t)), \quad \text{where } p_i(t) = \alpha_i - \delta\theta_i(t), \tag{8}$$

where α_i is the age-dependent base instantaneous infection probability of contact i, $\theta_i(t)$ is his/her status of vaccination at time t (taken as 0 or 1), and δ is the vaccine efficacy, measured in terms of the reduction in the base instantaneous infection probability (achieved after 10 days; Pasteur 2009). Note that, as $p_i(t)$ increases, the instantaneous force of infection $\lambda_i(t)$ grows at an increasing rate (see Fig. 6). The age-dependent base instantaneous infection probabilities were adopted from Germann et al. (2006) (see Appendix Table 10).

The disease natural history for H5N1 virus subtype was taken as the following: a latent period of 29 h, an incubation period of 46 h, and an infectiousness period between 29 and 127 h (Writing committee of the World Health Organization 2005).

The values of the base mortality probability of infected case i, μ_i (Eq. 3), were determined using the statistics recommended by the Working Group on Pandemic Preparedness and Influenza Response (Meltzer et al. 1999). These data show the percentage of mortality for age-based high-risk groups (see Appendix Table 11, columns 1–3). For the testbed scenario, the mortality probabilities for different age groups (Appendix Table 11, column 4) were estimated using the assumption that high-risk cases are expected to account for 85% of the total number of fatalities, for each age group (Meltzer et al. 1999).

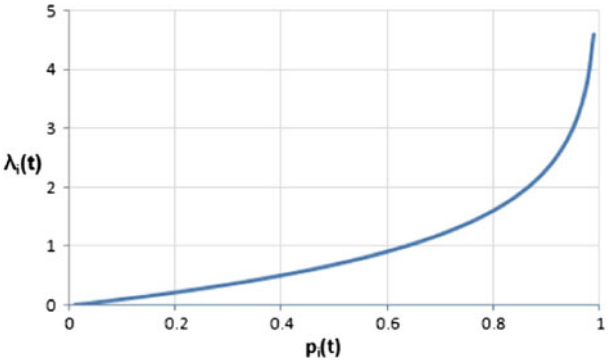

Fig. 6 $\lambda_i(t)$ versus $p_i(t)$

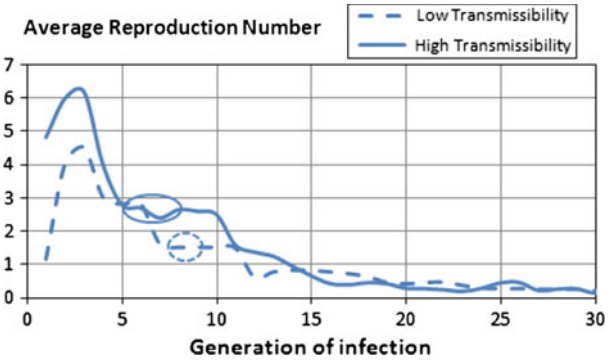

Fig. 7 Estimation of R_0 (Hillsborough)

4.1.2 Calibration of the single-region models

The single-region simulation models were calibrated against R_0 and IAR (see Sect. 3.3), using hourly contact rates within mixing groups. Original contact rates were adopted from Germann et al. (2006). These contact rates were adjusted to obtain the baseline values of R_0 similar to those estimated from past outbreaks (Ferguson et al. 2005; Mills et al. 2004), for both high and low transmissibility scenarios (see Appendix Table 12 for a sample of contact rates).

The values of R_0 were estimated for each region using the average reproduction numbers for generations of infection, as presented in Glass et al. (2006) and Ferguson et al. (2005), over multiple replicates (e.g., see Fig. 7 for the Hillsborough County). As the figure illustrates, generations 5 through 8 (the solid line) and generations 7 to 9 (the dotted line) represent "typical" (Glass et al. 2006) or representative infectious cases, born in the *early stage* of the pandemic, when most of the regional population is susceptible. For the purpose of computing the value of R_0, earlier generations were disregarded, as they were composed of a limited number of infected cases with highly variable individual reproduction numbers.

Historically, R_0 values for PI range between 1.4 and 3.9, where PI with $R_0 \leq 1.8$ are considered as of low transmissibility and PI with $2.2 \leq R_0 \leq 3.9$ as of high transmissibility (Ferguson et al. 2005; Mills et al. 2004). Henceforth, the R_0 value of 2.538 for the high transmissibility testbed (Fig. 7, solid line) and 1.525 for the low transmissibility testbed (Fig. 7, dotted line) were taken, for the Hillsborough County (other regions had similar R_0 values). These values corresponded to the simulated IARs of 0.881 and 0.538, respectively. Note that from the theoretical relationship in Eq. 4, IAR of 0.881 and 0.538 yield R_0 of 2.426 and 1.435, respectively. Thus, the simulated R_0 numbers show a good match with the theoretical approximations.

4.1.3 Mitigation-related parameters

The mitigation resources considered in the testbed included stockpiles of vaccines and antiviral, administration capacities for vaccination and antiviral therapy, and quarantine enforcement resources (required to achieve a targeted social distancing conformance level). We assumed a 24-h CDC resource deployment delay once the first infection case is confirmed (Centers for Disease Control and Prevention 2006).

Pharmaceutical measures The vaccination risk group included individuals younger than 5 years and older than 65 years (World Health Organization 2004). The risk group for antiviral application included individuals below 15 years and above 55 years (World Health Organization 2004; Institute of Medicine 2008). The efficacy levels for the vaccine δ (in Eq. 8) and antiviral τ (in Eq. 3) were assumed to be 40% (Longini et al. 2005; Treanor et al. 2006) and 30%, respectively. See Sect. 4.2.2 for a sensitivity analysis on both parameters. We assumed a 95% target population conformance for both measures. The immunity development period for the vaccine was taken as 10 days (Pasteur 2009); the antiviral was assumed to become effective immediately. Table 13 summarizes vaccination and antiviral treatment resource requirements for each region along with resource costs (PayScale 2009; Centers for Disease Control and Prevention 2009; PharmacyChecker.com 2009) and the total budget requirement.

Non-pharmaceutical measures A simplified version of the CDC guidance for non-pharmaceutical interventions for Category 5 was implemented (see Sect. 3.2.4, Centers for Disease Control and Prevention 2007b). Once the CFR has reached 1.0% in the affected region, a social distancing policy is declared and remains in effect for 14 days (Centers for Disease Control and Prevention 2007b). Individuals below a prespecified age ξ (22 years) were assumed to stay at home during the quarantine period. Of the remaining population, a certain proportion ϕ (Blendon et al. 2006) stayed at home and was allowed a 1-h leave, every 3 days, to buy essential supplies. The remaining $(1-\phi)$ non-compliant proportion followed a regular schedule. All testbed scenarios considered the quarantine conformance level ϕ (a decision variable) bounded between 50 and 80% (Colorado Department of Human Services Division of Mental Health 2009; Blendon et al. 2006).

An outbreak was considered contained, if the daily new infections did not exceed five cases, for seven consecutive days. Once contained, a region was simulated for an additional 10 days (Svensson 2007) to allow an accurate estimation of the pandemic statistics. The costs of lost productivity and medical expenses were adopted

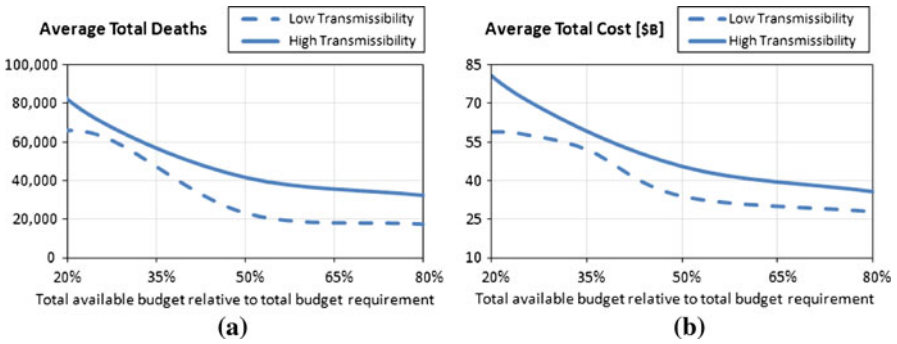

Fig. 8 Sensitivity analysis on total budget availability (measured in terms of the average number of deaths (**a**) and the average total cost (**b**))

from Meltzer et al. (1999) and inflation-adjusted using Halfhill (2009) (see Appendix Table 14). The medical costs of uninfected arising from the use of face masks and preventive medicine were not considered.

The optimization model was based on regression equations re-estimated at every outbreak epoch. For each region, we developed a 2^5 statistical design of experiment, to estimate the regression coefficients of the significant decision variables (factors) and their interactions. To ease the very significant computational burden, the testbed implementation considered allocation decisions only for new outbreak regions. The simulation code was written in C++ and run on a Pentium IV with a 3.40 GHz CPU and 4.0 GB RAM. The running time for a cross-regional simulation replicate averaged 20 min.

4.2 Sensitivity analysis

This section presents a sensitivity analysis for assessing the marginal impact of changes in the total budget availability and variability of some of the critical factors, for both low and high transmissibility scenarios. The marginal impact was measured separately by the change in the total pandemic cost and the number of mortalities (averaged over multiple replicates), resulting from a unit change in the total budget availability or a factor value, one at a time. Factors under consideration included: (a) antiviral efficacy, (b) vaccine efficacy, (c) social distancing conformance, (d) social distancing declaration threshold, and (e) social distancing period. We also investigated the affect of varying the social distancing conformance on the dynamics of the societal and economic costs.

4.2.1 Total budget availability

Figure 8a and b shows the dynamics of the pandemic impact, measured as the average number of fatalities and total cost, for different levels of the total budget availability relative to the total budget requirement (see Appendix Table 13).

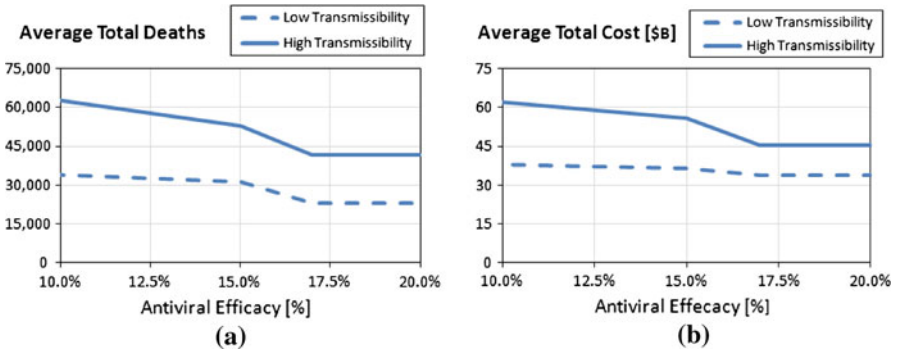

Fig. 9 Sensitivity analysis on antiviral efficacy (measured in terms of the average number of deaths (**a**) and the average total cost (**b**))

As expected, the curves for the average number of deaths and total cost exhibit a downward trend, for both transmissibility scenarios, as the total budget availability increases. An increased budget translates into higher availabilities of mitigation resources, which will mediate regional pandemic impact and reduce the probability of spread to unaffected regions. As also expected, a higher virus transmissibility generates more infections which, in turn, result into more fatalities and, subsequently, bigger societal and economic costs. As the budget availability approaches the budget requirement (starting from approximately 60%), both impact curves show a converging behavior, for both scenarios, whereby the marginal impact of additional resource availability decreases. This can be explained by noting that the total budget requirement was calculated assuming the worst case scenario where *all* regions are affected and provided with adequate resources to cover their respective populations at risk.

4.2.2 Antiviral efficacy

Figure 9a and b shows the behavior of the two impact measures for the level of the antiviral efficacy (τ in Eq. 3) between 10 and 20, and a fixed level of the total budget availability (50% of the total requirement).

As expected from Eq. 3, for both transmissibility scenarios, the two curves exhibit a decreasing trend which is approximately linear in the range of τ between 10 and 15%. As the value of τ approaches the value of the maximum base mortality probability (approximately 16% for the elderly risk group), the resultant effective mortality probability tends to zero, which explains the converging behavior of the curve representing the total number of mortalities. The total cost curve exhibits a similar pattern.

4.2.3 Vaccine efficacy

Both impact measure curves exhibit a downward trend as the vaccine efficacy (δ in Eq. 8) increases between 20 and 35%, with a fixed level of the total budget availability (50% of the total requirement; see Fig. 10a, b). For lower transmissibility, the marginal utility of the vaccine efficacy is less significant which can be explained by noting that

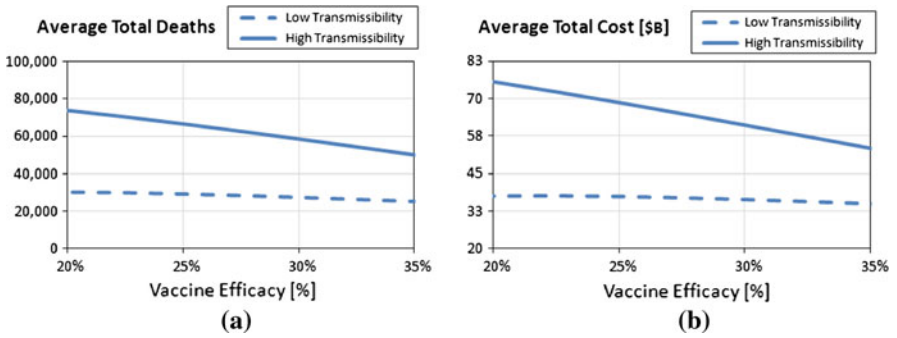

Fig. 10 Sensitivity analysis on vaccine efficacy (measured in terms of the average number of deaths (**a**) and the average total cost (**b**))

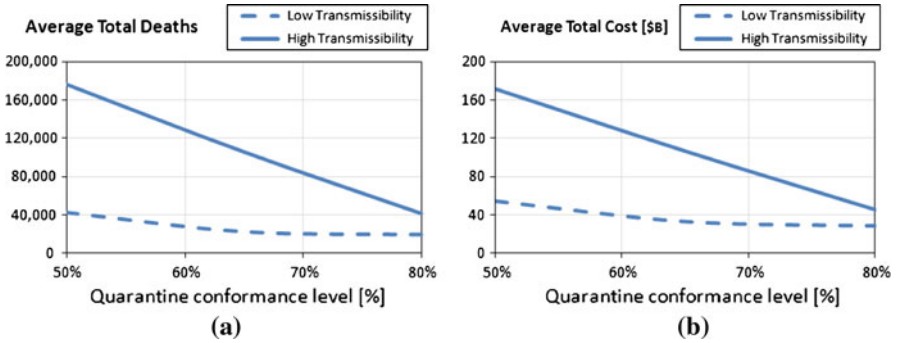

Fig. 11 Sensitivity analysis on social distancing conformance (measured in terms of the average number of deaths (**a**) and the average total cost (**b**))

such scenarios generate fewer infections and consequently, the overall impact of a more effective vaccine is less pronounced.

4.2.4 Social distancing conformance level

Reduction of the contact intensity through social distancing has long proven to be one of the most efficient mitigation mechanisms. Figure 11a and b shows the dynamics of the average number of fatalities and total cost for different levels of the social distancing conformance. The analysis was conducted for conformance levels between 50 and 80%.

For both transmissibility scenarios, the two curves exhibit a downward trend, which can be attributed to a reduced contact intensity associated with higher conformance. The trends are steeper for higher transmissibility scenarios which are characterized by more intensive social dynamics within the mixing groups. The reduction in the contact intensity gets amplified throughout generations of infection within the affected region and, more importantly, leads to reduced probabilities of spread to unaffected regions.

Figure 12a and b shows the dynamics of the total cost broken into the societal and economic components. The societal cost for the two scenarios generally decreases

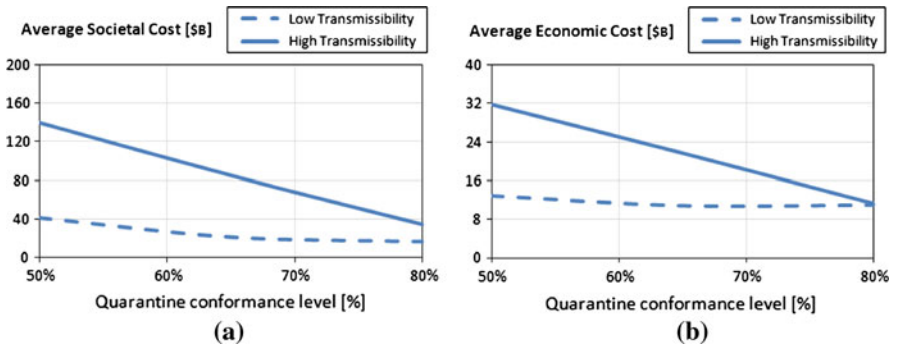

Fig. 12 Sensitivity analysis on social distancing conformance (societal (**a**) and economic cost (**b**))

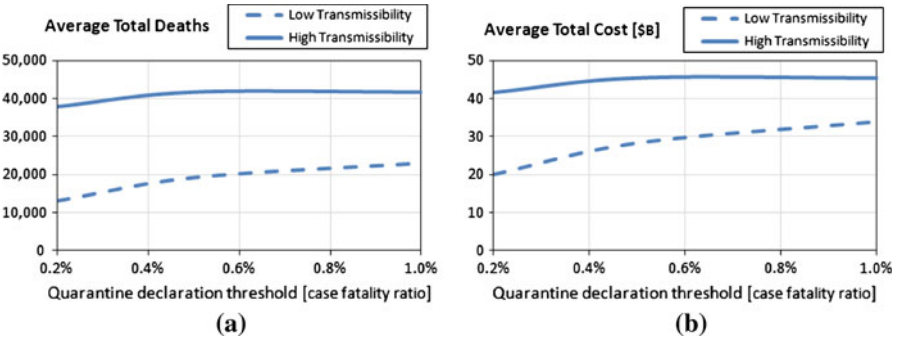

Fig. 13 Sensitivity analysis on social distancing declaration threshold (measured in terms of the average number of deaths (**a**) and the average total cost (**b**))

with quarantine conformance as a consequence of generating fewer infections and deaths (and hence, smaller lost productivity) during the quarantine period. For higher transmissibility, the marginal impact of the conformance level is more pronounced due to the effect of amplifying reduction in contact intensity explained above. A similar behavior can be observed for the economic cost which incorporates the cost of medical expenses of the recovered/deceased (over the entire pandemic period) and the cost of lost productivity of the quarantined individuals (during the social distancing period).

4.2.5 Social distancing declaration threshold

Figure 13a and b shows the dynamics of the impact measures for different levels of the social distancing declaration threshold, measured in terms of the CFR (see Sect. 4.1.3). The analysis was conducted for the CFR values between 0.2 and 1.0%.

For both scenarios, the trends are increasing since later declaration leads to a growth in the number of infected and dead. It can also be observed that for higher transmissibility, the curves reach saturation starting from CFR of approximately 0.55%. This can be explained by noting that in this case, the time difference in quarantine declaration using CFR values between 0.55 and 1.0 is insignificant.

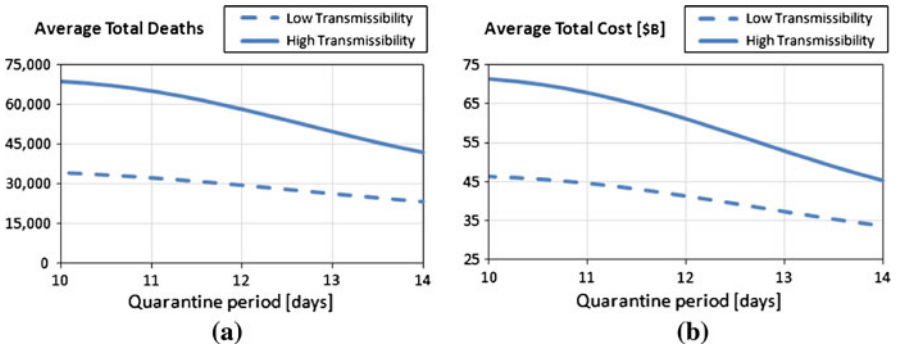

Fig. 14 Sensitivity analysis on social distancing period (measured in terms of the average number of deaths (**a**) and the average total cost (**b**))

4.2.6 Social distancing period

Figure 14a and b shows the dynamics of the average number of fatalities and total cost for values of the social distancing period between 10 and 14 days (Centers for Disease Control and Prevention 2007b). Similar to the analysis for the social distancing conformance level (see Sect. 4.2.4), for both transmissibility scenarios, the two curves exhibit a decreasing trend: once the CFR reaches a significant value of 1.0%, social distancing becomes the most efficient containment measure. From this point, any additional quarantine days (starting from 10 and up to 14 total days; Centers for Disease Control and Prevention 2007b) will reduce both the contact intensity during the quarantine period and also the size of the post-quarantine infectious population.

Based on our methodology, we have also developed a decision-aid simulator with a GUI which is made freely available to general public through our web site at http://imse.eng.usf.edu/pandemics.aspx. The simulator allows the input of data for regional demographic and social dynamics, and disease-related parameters (see Appendix Fig. 15). It is intended to assist public health decision makers in conducting customized what–if analysis for assessment of mitigation options and development of policy guidelines. Examples of such guidelines include targeted risk groups for vaccination and antiviral treatment, social distancing policies (e.g., thresholds for declaration and lifting, closure options (i.e., household-based, schools, etc.), and compliance targets), and guidelines for travel restrictions.

5 Conclusions

This paper presents a simulation-based optimization methodology for generating dynamic predictive mitigation strategies for pandemic outbreaks affecting several regions. The methodology can accommodate varying virus and population dynamics. It progressively allocates a limited budget to procure vaccines and antivirals, capacities for their administration, and resources required to enforce social distancing. The methodology uses measures of morbidity, mortality, and social distancing, which are translated into the costs of lost productivity and medical services. The methodology

was implemented on a mock outbreak and the efficacy of dynamic predictive resource allocation strategy was evaluated in comparison with the pro-rata allocation policy currently in use.

Summary of the main results For both low and high transmissibility scenarios under study, the marginal impact of additional resources on the policy performance reduced steadily. It was observed that while the total budget requirement was arrived at assuming that *all* regions would be affected, the dynamic predictive allocation strategy decreased the probability of spread from the ongoing regions, thus resulting in reduced need for resources. Our analysis also showed that compared to the high transmissibility scenario, marginal impact of the vaccine efficacy for the low transmissibility scenario was less significant due to a relatively smaller infected population. We observed that the overall pandemic cost was significantly affected by the social distancing conformance, particularly for higher transmissibility scenario. A higher degree of social distancing conformance led to a reduction in the contact intensity within the affected region. This further reduced the probabilities of spread to unaffected regions. We also observed that delayed declaration of social distancing led to a growth in the number of infected and dead. Moreover, for both transmissibility scenarios, longer social distancing period (from 10 to 14 days) significantly reduced the pandemic cost by decreasing both the contact intensity and the size of the post-quarantine infectious population.

Contributions of the paper To the best of our knowledge, our methodology is among the first to respond to IOM recommendations by developing a dynamic decision-aid tool, which incorporates both societal and economic impact measures. This paper makes the following contributions: (a) the model is capable of re-allocating resources remaining from the previous allocations and thus achieves a more efficient resource utilization; (b) the model incorporates the costs of the resources and aims to allocate a total available budget, as opposed to allocating available quantities of individual resources, which vary in their relative cost and effectiveness; (c) the testbed implementation considers optimal policy generation under both low and high transmissibility scenarios; (d) the paper investigates the dynamics of the societal and economic costs under varying social distancing policies. The simulation model features a flexible design which can be particularized to an even broader range of pharmaceutical and non-pharmaceutical interventions and more granular mixing groups. The methodology is intended to assist public health policy makers in developing dynamic strategies for allocation of limited resources during a pandemic outbreak involving multiple regions.

Acknowledgments We would like to acknowledge with thanks the many helpful suggestions made by Prof. Yiliang Zhu, Department of Epidemiology and Biostatistics at the University of South Florida, Tampa, FL, USA.

6 Appendix

See Tables 1, 2, 3, 4, 5, 6, 7, 8, 9, 10, 11, 12, 13, 14, and Fig. 15.

Table 1 A summary of simulation-based PI containment and mitigation models

Author (year)	Single region (SR)/ cross regional (CR)	Model objective	Key features
Ferguson et al. (2005, 2006)	SR (Thailand, 2005), SR (USA & UK, 2006)	Model PI spread & assess mitigation strategies	85M Thailand, 300M USA, 58.1M UK Use of GIS (Landscan) Use of targeted mass prophylaxis and social distancing A set of homogeneous mixing groups
Glass et al. (2006)	SR (small town in New Mexico, USA)	Examine role of social distancing	Targeted social distancing Fixed, small-scale contact network Time between infection events follows an exponential distribution
Germann et al. (2006)	SR (USA)	Assess mitigation strategies	281M inhabitants (2000 US census data) divided in 2000-person communities Sensitivity analysis on R_0 from 1.6 to 2.4
Wu et al. (2006b)	SR (Hong Kong)	Test different intervention scenarios	Natural history includes pre-symptomatic cases Use of household-based interventions Need for significant stocks of antiviral drugs
Colizza et al. (2006, 2007)	CR (global)	Model worldwide spread of a pandemic	Use of an air travel network Diverse urban centers Use of compartmental models (SLIR) Analysis of antiviral and travel restrictions
Halloran et al. (2008)	SR (Chicago)	Cross-validate targeted layered containment models (Ferguson/Germann/Eubank)	8.6 M people R_0 from 1.9 to 3.0 Assessment of intervention strategies
Cooley et al. (2008)	SR (North Carolina, USA)	Compare a simulated pandemic curve against real-life data	Use of 2003–04 North Carolina data Use of ILI data to estimate model parameters

Table 1 continued

Author (year)	Single region (SR)/ cross regional (CR)	Model objective	Key features
Das and Savachkin (2008)	SR	Mimic stochastic propagation of PI and assess mitigation strategies	Large-scale model (1.1M) Detailed schedules for inhabitants Heterogeneous mixing groups
Savachkin et al. (2010b)	CR (Florida, USA)	Model PI spread & assess comprehensive dynamic mitigation strategies	Dynamic predictive large-scale simulation-based optimization methodology 4M people testbed Use of vaccination, prophylaxes, and social distancing
Eclipse (2009)	CR (global)	Model worldwide PI spread	Geographic visualization of PI spread Use of SIR model Limited to land transportation

Table 2 Distribution of regional adult population by age (US Census Bureau 2000)

Age group/Region	Adult population distribution by age			
	Hillsborough	Miami Dade	Duval	Leon
23–29	0.16	0.15	0.16	0.24
30–64	0.67	0.66	0.69	0.63
65–99	0.17	0.19	0.15	0.13

Table 3 Distribution of regional children population by age (US Census Bureau 2000)

Age group/Region	Children population distribution by age			
	Hillsborough	Miami Dade	Duval	Leon
0–5 (pre-school)	0.24	0.22	0.24	0.16
6–9 (elementary school)	0.23	0.23	0.25	0.17
10–14 (middle school)	0.25	0.25	0.23	0.17
15–17 (high school)	0.13	0.14	0.14	0.10
18–22 (college)	0.15	0.16	0.14	0.40

Table 4 Distribution of regional population by households (US Census Bureau 2000)

Household type		Regional population by household type			
# Adults	# Children	Hillsborough	Miami Dade	Duval	Leon
1	0	0.28	0.25	0.27	0.30
1	1	0.04	0.04	0.04	0.04
2	0	0.31	0.26	0.30	0.32
1	2	0.04	0.05	0.05	0.04
2	1	0.13	0.15	0.14	0.13
1	3	0.01	0.01	0.01	0.01
2	2	0.13	0.15	0.13	0.11
1	4	0.01	0.01	0.01	0.00
2	3	0.06	0.08	0.06	0.04

Table 5 Composition of mixing groups, Hillsborough County (Bureau of Transportation Statistics 2002)

Mixing group (MG) type	Number of MG	Distribution of workplaces	Distribution of weekday errands	Distribution of weekend errands	Distribution of quarantine errands	Hourly contact rate
Home	1	0.066	0.000	0.000	0.800	1.500
Factory	613	0.058	0.000	0.000	0.000	0.750
Office	2,266	0.302	0.000	0.000	0.000	0.750
Pre-school	224	0.005	0.000	0.000	0.000	1.050
Elementary school	66	0.010	0.000	0.000	0.000	2.573
Middle school	134	0.203	0.000	0.000	0.000	3.750
High school	59	0.097	0.000	0.000	0.000	3.750
College	46	0.106	0.000	0.000	0.000	3.750
Afterschool center	256	0.007	0.000	0.000	0.000	1.500
Grocery store	390	0.026	0.619	0.515	0.100	0.375
Restaurant	223	0.087	0.278	0.256	0.000	0.375
Entertainment center	360	0.032	0.066	0.116	0.000	0.375
Church	86	0.001	0.037	0.113	0.100	0.375

Table 6 Composition of mixing groups, Miami Dade County (Bureau of Transportation Statistics 2002)

Mixing group (MG) type	Number of MG	Distribution of workplaces	Distribution of weekday errands	Distribution of weekend errands	Distribution of quarantine errands	Hourly contact rate
Home	1	0.092	0.000	0.000	0.800	1.500
Factory	1,353	0.035	0.000	0.000	0.000	0.750
Office	2,880	0.128	0.000	0.000	0.000	0.750
Pre-school	188	0.010	0.000	0.000	0.000	1.050
Elementary school	246	0.188	0.000	0.000	0.000	2.573
Middle school	84	0.098	0.000	0.000	0.000	3.750
High school	82	0.116	0.000	0.000	0.000	3.750
College	59	0.206	0.000	0.000	0.000	3.750
Afterschool center	507	0.006	0.000	0.000	0.000	1.500
Grocery store	942	0.025	0.619	0.515	0.100	0.375
Restaurant	3,935	0.085	0.278	0.255	0.000	0.375
Entertainment center	758	0.011	0.066	0.116	0.000	0.375
Church	266	0.000	0.037	0.113	0.100	0.375

Table 7 Composition of mixing groups, Duval County (Bureau of Transportation Statistics 2002)

Mixing group (MG) type	Number of MG	Distribution of workplaces	Distribution of weekday errands	Distribution of weekend errands	Distribution of quarantine errands	Hourly contact rate
Home	1	0.049	0.000	0.000	0.800	1.500
Factory	519	0.063	0.000	0.000	0.000	0.750
Office	2,880	0.313	0.000	0.000	0.000	0.750
Pre-school	74	0.006	0.000	0.000	0.000	1.050
Elementary school	116	0.170	0.000	0.000	0.000	2.572
Middle school	35	0.083	0.000	0.000	0.000	3.750
High school	30	0.087	0.000	0.000	0.000	3.750
College	21	0.112	0.000	0.000	0.000	3.750
Afterschool center	245	0.006	0.000	0.000	0.000	2.000
Grocery store	320	0.024	0.619	0.515	0.100	1.500
Restaurant	1,474	0.074	0.278	0.255	0.000	0.375
Entertainment center	244	0.012	0.066	0.116	0.000	0.375
Church	77	0.001	0.037	0.113	0.100	0.375

Table 8 Composition of mixing groups, Leon County (Bureau of Transportation Statistics 2002)

Mixing group (MG) Type	Number of MG	Distribution of workplaces	Distribution of weekday errands	Distribution of weekend errands	Distribution of quarantine errands	Hourly contact rate
Home	1	0.072	0.000	0.000	0.800	1.50
Factory	103	0.012	0.000	0.000	0.000	0.750
Office	1,093	0.212	0.000	0.000	0.000	0.750
Pre-school	20	0.008	0.000	0.000	0.000	1.050
Elementary school	30	0.106	0.000	0.000	0.000	2.573
Middle school	15	0.051	0.000	0.000	0.000	3.750
High school	14	0.064	0.000	0.000	0.000	3.750
College	9	0.374	0.000	0.000	0.000	3.750
Afterschool center	60	0.005	0.000	0.000	0.000	1.500
Grocery store	52	0.021	0.619	0.515	0.100	0.375
Restaurant	512	0.069	0.278	0.255	0.000	0.375
Entertainment center	73	0.006	0.066	0.116	0.000	0.375
Church	16	0.002	0.037	0.113	0.100	0.375

Table 9 Inter-regional travel probabilities (Tampa International Airport 2010; Miami International Airport 2010; Jacksonville Aviation Authority 2010; Tallahassee Regional Airport 2010)

Origin/Destination	Inter-regional travel probability			
	Hillsborough	Miami Dade	Duval	Leon
Hillsborough	0.00	0.60	0.27	0.13
Miami Dade	0.74	0.00	0.16	0.10
Duval	0.61	0.29	0.00	0.10
Leon	0.52	0.31	0.17	0.00

Table 10 Instantaneous infection probability for different age groups: adopted from Germann et al. (2006)

Age group	0–5	6–19	20–29	31–65	66–99
α_i	0.156	0.106	0.205	0.195	0.344

Table 11 Mortality probability for different age groups (Meltzer et al. 1999)

Age group	% High-risk cases	% Death for high-risk cases	Mortality probability
0–19	6.4	9.0	0.007
20–64	14.4	40.9	0.069
65+	40.0	34.4	0.162

Table 12 Hourly contact rates by mixing group (Hillsborough County, high transmissibility scenario): adopted from Germann et al. (2006)

Mixing group	Hourly contact rate
Home	1.50
Factory	0.75
Office	0.75
Preschool	1.05
Elementary school	2.57
Middle school	3.75
High school	3.75
University	3.75
Afterschool center	1.50
Grocery store	0.38
Restaurant	0.38
Entertainment center	0.38
Church	0.38

Table 13 Regional resource and budget requirements (PayScale 2009; Centers for Disease Control and Prevention 2009; PharmacyChecker.com 2009)

Region (population)	Resource Requirements by region					Cost of Resource	Required budget by Resource
	Hillsb. (1,007,916)	Miami D. (2,209,702)	Duval (852,168)	Leon (248,761)	Total (4,318,547)		
Resource							
Vaccine stock	305,036	679,181	241,522	76,007	1,301,745	$8.48/dose	$11,038,800
Antiviral stock	415,294	749,058	460,393	105,307	1,730,052	$60/dose	$103,803,140
No. of nurses (antiv.)	650	1,104	786	166	2,706	$27/h, 8 h/day, 50 days	$29,226,975
No. of nurses (vacc.)	1,059	2,358	839	264	4,520	$27/h, 8 h/day, 14 days	$13,668,326
Total budget requirement							$157,737,241

Table 14 Values of pandemic impact measures (societal and economic costs; Meltzer et al. 1999; Halfhill 2009)

Pandemic impact measure (age group, years)	Value US$
Average cost of lost lifetime productivity of a deceased case (0–19)	$1,336,347.86
Average cost of lost lifetime productivity of a deceased case (20–64)	$1,370,987.28
Average cost of lost lifetime productivity of a deceased case (65–99)	$98,959.24
Average cost of lost productivity and medical expenses of a recovered/deceased case (0–19)	$5,078.48
Average cost of lost productivity and medical expenses of a recovered/deceased case (20–64)	$10,466.68
Average cost of lost productivity and medical expenses of a recovered/deceased case (65–99)	$11,566.09
Average daily cost of lost productivity of a non-infected quarantined case (20–99)	$432.54

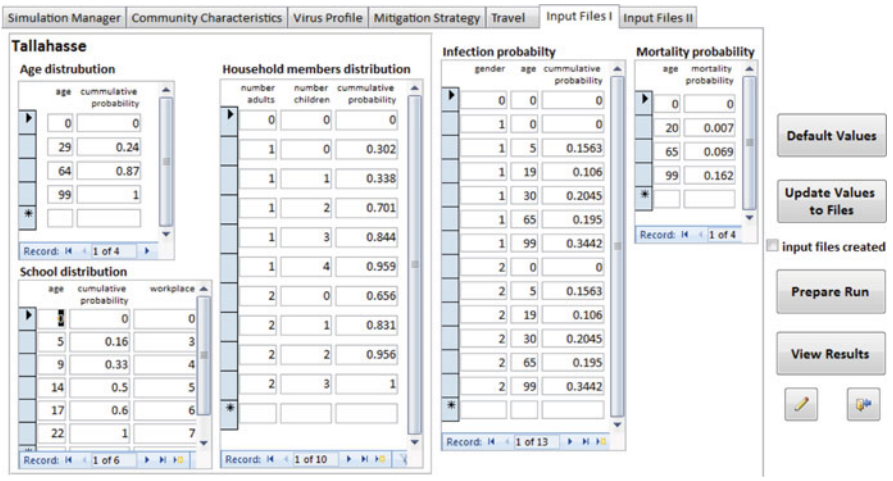

Fig. 15 A snapshot of the decision-aid simulator GUI

References

Arino J, Brauer F, den Driessche P, Watmough J, Wu J (2006) Simple models for containment of a pandemic. J R Soc Interface 3:453–457

Atkinson M, Wein L (2008) Quantifying the routes of transmission for pandemic influenza. Bull Math Biol 70(3):820–867

Aunins J, Lee A, Volkin D (2000) Vaccine production, 2nd edn. CRC Press LLC, Boca Raton

Ball F, Lyne O (2002) Optimal vaccination policies for stochastic epidemics among a population of households. Math Biosci 177–178:333–354

Blendon R, DesRoches C, Cetron M, Benson J, Meinhardt T, Pollard W (2006) Attitudes toward the use of quarantine in a public health emergency in four countries. Health Aff 25(2):15–25

Blendon R, Koonin L, Benson J, Cetron M, Pollard W, Mitchell E, Weldon K, Herrmann M (2008) Public response to community mitigation measures for pandemic influenza. Emerg Infect Dis 14(5):778

Bootsma M, Ferguson N (2007) The effect of public health measures on the 1918 influenza pandemic in the US cities. PNAS 104(18):7588–7593

Brundage J, Shanks G (2008) Deaths from bacterial pneumonia during 1918–19 influenza pandemic. Emerg Infect Dis 14(8):1193

Bureau of Transportation Statistics (2002) 2001 National household travel survey (NTHS). http://www.bts.gov/programs/national_household_travel_survey/. Last accessed on 12/09/2008

Carrat F, Lavenu A, Cauchemez S, Deleguer S (2005) Repeated influenza vaccination of healthy children and adults: borrow now, pay later? Epidemiol Infect 134:63–70

Cauchemez S, Carrat F, Viboud C, Valleron A, Boelle P (2004) A Bayesian (MCMC) approach to study transmission of influenza: application to household longitudinal data. Stat Med 23:3469–3487

Centers for Disease Control and Prevention (CDC) (2006) CDC influenza operational plan. http://www.cdc.gov/flu/pandemic/cdcplan.htm. Last accessed on 03/27/2009

Centers for Disease Control and Prevention (CDC) (2007a) Preparing for pandemic influenza. http://www.cdc.gov/flu/pandemic/preparedness.htm. Last accessed on 04/27/2009

Centers for Disease Control and Prevention (CDC) (2007b) Interim pre-pandemic planning guidance: community strategy for pandemic influenza mitigation in the United States. http://www.pandemicflu.gov/plan/community/community_mitigation.pdf. Last accessed on 04/01/2009

Centers for Disease Control and Prevention (CDC) (2008) Avian influenza: current H5N1 situation. http://www.cdc.gov/flu/avian/outbreaks/current.htm#clusters. Last accessed on 02/09/2008

Centers for Disease Control and Prevention (2009) CDC vaccine price list. http://www.cdc.gov/vaccines/programs/vfc/cdc-vac-price-list.htm#flu. Last accessed on 12/28/2009

Colorado Department of Human Services Division of Mental Health (2009) Pandemic influenza: quarantine, isolation and social distancing. http://www.flu.gov/news/colorado_toolbox.pdf. Last accessed on 10/28/2009

Colizza V, Barrat A, Barthelemy M, Vespignani A (2006) The role of the airline transportation network in the prediction and predictability of global epidemics. PNAS 103:2015–2020

Colizza V, Barrat A, Barthelemy AVM, Vespignani A (2007) Modeling the worldwide spread of pandemic influenza: baseline case and containment interventions. PLOS Med 4:95–110

Committee on Modeling Community Containment for Pandemic Influenza (2006) Modeling community containment for pandemic influenza: a letter report. http://www.nap.edu/catalog/11800.html. Last accessed on 12/09/2008

Cooley P, Ganapathi L, Ghneim G, Holmberg S, Wheaton W, Hollingsworth C (2008) Using influenza-like illness data to reconstruct an influenza outbreak. Math Comput Model 48:929–939

Cummings K, Jette A, Brock B, Haefner D (1979) Psychosocial determinants of immunization behavior in a swine influenza campaign. Med Care 17(6):639–649

Dargatz C, Georgescu V, Held L (2006) Stochastic modelling of the spatial spread of influenza in Germany. Austrian J Stat 35(1):5–20

Das T, Savachkin A (2008) A large scale simulation model for assessment of societal risk and development of dynamic mitigation strategies. IIE Trans 40(9):893–905

Diekmann O, Heesterbeek J (2000) Mathematical epidemiology of infectious diseases: model building, analysis and interpretation. Wiley, Chichester

Eclipse F (2009) The spatio-temporal epidemiological modeler. http://www.eclipse.org/stem/intro.php. Last accessed on 11/06/2009

Epstein J, Goedecke D, Yu F, Morris R, Wagener D, Bobashev G (2007) Controlling pandemic flu: the value of international air travel restrictions. PLoS One 2(5):1–11

Epstein J, Parker J, Cummings D, Hammond R (2008) Coupled contagion dynamics of fear and disease: mathematical and computational explorations. PLoS One 3(12):e3955

Eubank S, Guclu H, Kumar V, Marathe M, Srinivasan A, Toroczkai Z, Wang N (2004) Modelling disease outbreaks in realistic urban social networks. Nature 429:180–184

Fedson D, Hant S (2003) Pandemic influenza and the global vaccine supply. Clin Infect Dis 36:1552–1561

Ferguson N, Mallett S, Jackson H, Roberts N, Ward P (2003) A population-dynamic model for evaluating the potential spread of drug-resistant influenza virus infections during community-based use of antivirals. J Antimicrob Chemother 51:977–990

Ferguson NM, Cummings D, Cauchemez S, Fraser C, Riley S, Aronrag M, Lamsirithaworn S, Burke D (2005) Strategies for containing an emerging influenza pandemic in Southeast Asia. Nature 437:209–214

Ferguson N, Cummings DA, Fraser C, Cajka J, Cooley PCC, Burke DS (2006) Strategies for mitigating an influenza pandemic. Nature 442(27):448–452

Fraser C, Riley S, Anderson R, Ferguson N, May R (2004) Factors that make an infectious disease outbreak controllable. PNAS 101(16):6146–6151
Germann T, Kadau K, Longini IM, Macken C (2006) Mitigation strategies for pandemic influenza in the United States. PNAS 103:5935–5940
Glass R, Beyeler W, Min H (2006) Targeted social distancing design for pandemic influenza. Emerg Infect Dis 12(11):1671–1681
Halder N, Kelso J, Milne G (2010) Analysis of the effectiveness of interventions used during the 2009 A/H1N1 influenza pandemic. BioMed Central 10(168):1–14
Halfhill T (2009) Inflation calculator. http://www.halfhill.com/inflatation.html. Last accessed on 12/04/2009
Halloran M (2006) Invited commentary: challenges of using contact data to understand acute respiratory disease transmission. Am J Epidemiol 164(10):945
Halloran ME, Longini IM, Nizam A, Yang Y (2002) Containing bioterrorist smallpox. Science 298:1428–1432
Halloran ME, Ferguson NM, Eubank S, Longini I (2008) Modeling targeted layered containment of an influenza pandemic in the United States. PNAS 105(12):4639–4644
Handel A, Longini I, Antia R (2009) Towards a quantitative understanding of the within-host dynamics of influenza A infections. Epidemics 1(3):185–195
HHS (2007) Pandemic planning update iv. http://www.pandemicflu.gov/plan/panflureport4.html
Institute of Medicine (IOM) (2008) Antivirals for pandemic influenza: guidance on developing a distribution and dispensing program. The National Academies Press, Washington, DC
Jacksonville Aviation Authority: daily traffic volume data (2010) http://www.jaa.aero/General/Default.aspx. Last accessed on 04/07/2010
Keane M, Walter M, Patel B, Moorthy S, Stevens R, Bradley K, Buford J, Anderson E, Anderson L, Tibbals K (2005) Confidence in vaccination: a parent model. Vaccine 23(19):2486–2493
Kelso J, Milne G, Kelly H (2009) Simulation suggests that rapid activation of social distancing can arrest epidemic development due to a novel strain of influenza. BMC Public Health 9(1):1–10
Larson R (2007) Simple models of influenza progression within a heterogeneous population. Oper Res 55(399–412):165–195
Lawless J, Lawless J (1982) Statistical models and methods for lifetime data. Wiley, New York
Lipsitch M, Cohen T, Murray M, Levin B (2007) Antiviral resistance and the control of pandemic influenza. PLoS Med 4(1):111–115
Longini IM (1986) The generalized discrete-time epidemic model with immunity: a synthesis. Math Biosci 82:19–41
Longini IM, Koopman JS (1982) Household and community transmission parameters from final distributions of infections in households. Biometrics 38:115–126
Longini IM, Halloran ME, Nizam A, Yang Y (2004) Containing pandemic influenza with antiviral agents. Am J Epidemiol 159(7):623–633
Longini IM, Nizam A, Shufu X, Ungchusak K, Hanshaoworakul W, Cummings D, Halloran ME (2005) Containing pandemic influenza at the source. Science 309:1083–1087
Maunder R, Hunter J, Vincent L, Bennett J, Peladeau N, Leszcz M, Sadavoy J, Verhaeghe L, Steinberg R, Mazzulli T (2003) The immediate psychological and occupational impact of the 2003 SARS outbreak in a teaching hospital. Can Med Assoc J 168(10):1245–1251
Meltzer M, Cox N, Fukuda K (1999) The economic impact of pandemic influenza in the United States: priorities for intervention. Emerg Infect Dis 5(5):659–671
Miami International Airport: daily traffic volume data (2010) http://www.miami-airport.com. Last accessed on 04/07/2010
Mills C, Robins J, Lipsitch M (2004) Transmissibility of 1918 pandemic influenza. Nature 432:904–906
Milne G, Kelso J, Kelly H, Huband S, McVernon J (2008) A small community model for the transmission of infectious diseases: comparison of school closure as an intervention in individual-based models of an influenza pandemic. PLoS One 3(12):1–7
Niederhauser V, Baruffi G, Heck R (2001) Parental decision-making for the varicella vaccine. J Pediatr Health Care 15(5):236–243
Nigmatulina KR, Larson RC (2009) Living with influenza: impacts of government imposed and voluntarily selected interventions. Eur J Oper Res 195(6/1):613–627
Ortutay B (2010) How thermal-imaging cameras spot flu fevers. http://www.msnbc.msn.com/id/30523865/. Last accessed on 03/19/2010

Pasteur S (2009) Influenza A(H1N1) 2009 monovalent vaccine. http://www.fda.gov/downloads/biologicsbloodvaccines/vaccines/approvedproducts/ucm182404.pfd. Last accessed on 11/18/2009

Patel R, Longini I, Halloran M (2005) Finding optimal vaccination strategies for pandemic influenza using genetic algorithms. J Theor Biol 234:201–212

PayScale (2009) Job: registered nurse (rn). http://www.payscale.com/rcsearch.aspx?country=US&str=Registered+Nurse+. Last accessed on 12/28/2009

Pearson M, Bridges C, Harper S (2006) Influenza vaccination of health-care personnel. Recommendations of the Healthcare Infection Control Practices Advisory Committee (HICPAC) and the Advisory Committee on Immunization Practices (ACIP) [Internet]. Last accessed on 10/28/2009

PharmacyChecker.com (2009) Pricing & ordering comparisons. http://www.pharmacychecker.com/Pricing.asp?DrugId=36260&DrugStrengthId=61300&sortby=Price. Last accessed on 12/28/2009

Pitzer V, Olsen S, Bergstrom C, Dowell S, Lipsitch M (2007a) Little evidence for genetic susceptibility to influenza A (H5N1) from family clustering data. Emerg Infect Dis 13(7):1074–1076

Pitzer V, Leung G, Lipsitch M (2007b) Estimating variability in the transmission of severe acute respiratory syndrome to household contacts in Hong Kong, China. Am J Epidemiol 166(3):355–359

Pourbohloul B, Ahued A, Davoudi B, Meza R, Meyers L, Skowronski D, Villaseñor I, Galván F, Cravioto P, Earn D et al (2009) Initial human transmission dynamics of the pandemic (H1N1) 2009 virus in North America. Influenza Other Respir Viruses 3(5):215–222

Rhodes S, Hergenrather K (2002) Exploring hepatitis B vaccination acceptance among young men who have sex with men: facilitators and barriers. Prevent Med 35(2):128–134

Robertson E, Hershenfield K, Grace S, Stewart D (2004) The psychosocial effects of being quarantined following exposure to SARS: a qualitative study of Toronto health care workers. Can J Psychiatry 49:403–407

Rosenthal S, Kottenhahn R, Biro F, Succop P (1995) Hepatitis B vaccine acceptance among adolescents and their parents. J Adolesc Health 17(4):248–255

Sadique M, Edmunds W, Smith R, Meerding W, de Zwart O, Brug J, Beutels P (2007) Precautionary behavior in response to perceived threat of pandemic influenza. Emerg Infect Dis 13(9):1307

Safranek T, Lawrence D, Kuriand L, Culver D, Wiederholt W, Hayner N, Osterholm M, O'Brien P, Hughes J (1991) Reassessment of the association between Guillain-Barré syndrome and receipt of swine influenza vaccine in 1976–1977: results of a two-state study. Am J Epidemiol 133(9):940

Savachkin A, Uribe-Sánchez A, Das T, Prieto D, Santana A, Martinez D (2010a) Supplemental data and model parameter values for cross-regional simulation-based optimization testbed. http://imse.eng.usf.edu/pandemic/supplement.pdf. Last accessed on 04/15/2010

Savachkin A, Uribe A, Das T, Prieto D (2010b) Developing dynamic predictive strategies for mitigation of cross-regional pandemic outbreaks. IIE Trans (in review)

Scharfstein D, Halloran M, Chu H, Daniels M (2006) On estimation of vaccine efficacy using validation samples with selection bias. Biostatistics 7(4):615

Schoenstadt A (2009) Spanish flu. http://flu.emedtv.com/spanish-flu/spanish-flu.html. Last accessed on 12/15/2009

Smailbegovic M, Laing G, Bedford H (2003) Why do parents decide against immunization? The effect of health beliefs and health professionals. Child Care Health Dev 29(4):303

Svensson A (2007) A note on generation times in epidemic models. Math Biosci 208(1):300–311

Treanor J, Campbell J, Zangwill K, Rowe T, Wolff M (2006) Safety and immunogenicity of an inactivated subvirion influenza A(H5N1) vaccine. N Engl J Med 3554(13):1343

Tallahassee Regional Airport: daily traffic volume data (2010) http://www.talgov.com/airport/index.cfm. Last accessed on 04/07/2010

Tampa International Airport: daily traffic volume data (2010) http://www.tampaairport.com. Last accessed on 04/07/2010

Tang Y, Longini I, Halloran M (2006) Design and evaluation of prophylactic interventions using disease incidence data from close contact groups. Appl Stat 55(3):317–330

The New Yorker (2009) The fear factor. http://www.newyorker.com/talk/comment/2009/10/12/091012taco_talk_specter. Last accessed on 10/28/2009

The New York Times (2009) Doctors swamped by swine flu vaccine fears. http://www.msnbc.msn.com/id/33179695/ns/health-swine_flu/. Last accessed on 10/28/2009

Uribe A, Prieto D, Savachkin A, Das T, Zhu Y (2008) A cross-regional pandemic outbreak simulation model: an aid to national resource allocation policy making. In: Proceedings of the 3rd INFORMS workshop on data mining and health informatics (DM-DI 2008)

US Census Bureau (2000) 2001 American community survey. http://www.census.gov/prod/2001pubs/statab/sec01.pdf. Last accessed on 03/27/2009

US Department of Health & Human Services (2007) HHS pandemic influenza plan. http://www.hhs.gov/pandemicflu/plan/. Last accessed on 03/27/2009

WHO Global Influenza Programme (2009) Pandemic influenza preparedness and response. Tech. Rep. World Health Organization

World Health Organization (WHO) (2004) WHO guidelines on the use of vaccine and antivirals during influenza pandemics. http://www.who.int/csr/resources/publications/influenza/11_29_01_A.pdf. Retrieved 03/27/2009

World Health Organization (2009) Pandemic (h1n1) 2009 vaccine deployment update, 17 December 2009. http://www.who.int/csr/disease/swineflu/vaccines/h1n1_vaccination_deployment_update_20091217.pdf

World Health Organization (WHO) (2010a) Cumulative number of confirmed human cases of Avian Influenza A(H5N1) reported to WHO. http://www.who.int/csr/disease/avian_influenza/country/cases_table_2010_07_05/en/index.html

World Health Organization (2010b) Pandemic (H1N1) 2009—update 107. http://www.who.int/csr/don/2010_07_02/en/index.html. Last accessed on 07/08/2010

Writing Committee of the World Health Organization (WHO) (2005) Consultation on human influenza A/H5. Avian influenza A(H5N1) infection in humans. N Engl J Med 353(13):1374–1385

Wu JT, Riley S, Fraser C, Leung G (2006a) Spatial considerations for the allocation of pre-pandemic influenza vaccination in the United States. Proc R Soc Biol Sci 274(1627):2811–2817

Wu JT, Riley S, Fraser C, Leung G (2006b) Reducing the impact of the next influenza pandemic using household-based public health interventions. PLoS Med 3(9):1532–1540

Yang Y, Sugimoto J, Halloran M, Basta N, Chao D, Matrajt L, Potter G, Kenah E, Longini I Jr (2009a) The transmissibility and control of pandemic influenza A (H1N1) virus. Science 326(5953):729–733

Yang Y, Halloran M, Longini I Jr (2009b) A Bayesian model for evaluating influenza antiviral efficacy in household studies with asymptomatic infections. Biostatistics 10(2):390

Yang Y, Halloran M, Sugimoto J, Longini I Jr (2007) Detecting human-to-human transmission of avian influenza A (H5N1). Emerg Infect Dis 13(9):1348–1353

Yasuda H, Suzuki K (2009) Measures against transmission of pandemic H1N1 influenza in Japan in 2009: simulation model. Eur Commun Dis Bull [Euro surveillance: bulletin européen sur les maladies transmissibles] 14(44):1–7